Coherent and Dephasing Spectroscopy for Single-Impurity Probing of an Ultracold Bath

Daniel Adam, Quentin Bouton, Jens Nettersheim, Sabrina Burgardt, Artur Widera

Coherent and Dephasing Spectroscopy for Single-Impurity Probing of an Ultracold Bath

Daniel Adam,[1] Quentin Bouton,[1,2] Jens Nettersheim,[1] Sabrina Burgardt,[1] and Artur Widera[1,*]
[1]Department of Physics and Research Center OPTIMAS, Technische Universität Kaiserslautern, Kaiserslautern 67663, Germany
[2]Laboratoire de Physique des Lasers, CNRS, UMR 7538, Université Sorbonne Paris Nord, F-93430 Villetaneuse, France

(Received 10 May 2021; accepted 24 August 2022; published 15 September 2022)

We report Ramsey spectroscopy on the clock states of individual Cs impurities immersed in an ultracold Rb bath. We record both the interaction-driven phase evolution and the decay of fringe contrast of the Ramsey interference signal to obtain information about bath density or temperature nondestructively. The Ramsey fringe is modified by a differential shift of the collisional energy when the two Cs states superposed interact with the Rb bath. This differential shift is directly affected by the mean gas density and the details of the Rb-Cs interspecies scattering length, affecting the phase evolution and the contrast of the Ramsey signal. Additionally, we enhance the temperature dependence of the phase shift preparing the system close to a low-magnetic-field Feshbach resonance where the s-wave scattering length is significantly affected by the collisional (kinetic) energy. Analyzing coherent phase evolution and decay of the Ramsey fringe contrast, we probe the Rb cloud's density and temperature. Our results point at using individual impurity atoms as nondestructive quantum probes in complex quantum systems.

DOI: 10.1103/PhysRevLett.129.120404

Individual impurities immersed in a gas form a paradigm of open quantum systems. An application of this scenario, which has attracted significant interest in recent years, is quantum probing, where information of a many-body system is mapped nondestructively onto quantum states of the impurity [1–3]. A prominent example is thermometry of quantum gases, where precise temperature information is to be determined. Realizations of impurity-based quantum gas thermometry include mapping thermal information onto the classical motional state of ensembles of impurities [4–6], single impurities [7], or the impurities' quantum spin distribution [8]. These methods, however, either used classical degrees of freedom or inelastic processes, perturbing the many-body system either by exchange of energy or angular momentum. To reduce perturbations, advanced proposals suggest storing information about the gas in the phase of quantum superpositions of quasispin states in single atoms [9–15]. In the context of many-body physics, the spin coherence of neutral impurities in an ultracold gas has been studied [16,17]. Moreover, exploiting specific properties of the bath, which modify the nonequilibrium dynamics of the probe, can enhance quantum thermometry [18]. For a Bose-Einstein condensate, an impurity can form a polaronic quasiparticle, and thermal information can be obtained from fluctuations of the probes' momentum and position [19]. By contrast, in a Fermi gas, the existence of a Fermi sea allows deducing thermal information from the dephasing dynamics of a coherent superposition of internal probe states [20].

Here, we couple individual Cs atoms in a coherent superposition of the clock states to an ultracold bath of Rb atoms, see Fig. 1. We prepare the gas just above the critical condensate temperature, with temperatures in the range $T/T_c = 1.2$–5, with T_c the critical temperature. Despite a relatively large interspecies s-wave scattering length of

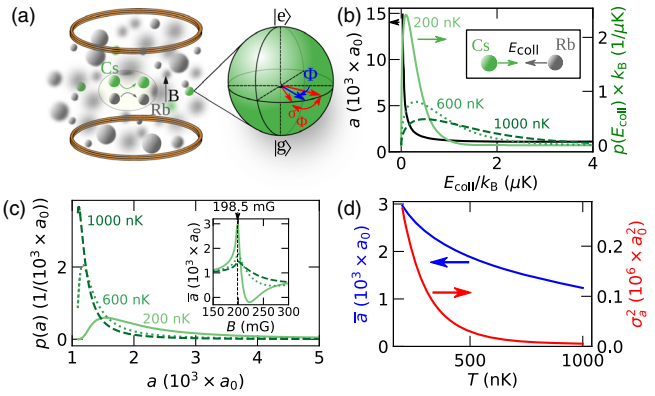

FIG. 1. (a) Single impurity (green) immersed in Rb bath (gray) interacting. The coherent superposition of Cs states is visualized on a Bloch sphere showing the interaction-induced phase evolution Φ and phase dispersion σ_Φ. (b) Scattering length a (black solid) for the Cs ground state $|g\rangle$ interacting with the Rb bath for different collision energies (inset) in the vicinity of a Feshbach resonance at 198.5 mG. On the same graph, we also plot the Maxwell-Boltzmann distribution of collision energies in green for 200, 600, and 1000 nK from light to dark green in solid, dotted, and dashed lines, respectively. (c) Probability distribution of the scattering length a for different bath temperatures; colors and line styles as in (b). Inset: a temperature-averaged scattering length $\bar{a}$ versus B field. The black dashed line marks the experimentally fixed magnetic field B at 198.50 ± 0.05 mG, at the peak of the Feshbach resonance. (d) Mean scattering length $\bar{a}$ (blue) as well as the variance of the probability distribution of scattering length σ_a^2 (red) as a function of temperature.

several thousand Bohr radii, see Fig. 1(b), our configuration leads to a Cs mean free path that is similar or larger than the Cs impurity's de Broglie wavelength. Therefore, our system differs from the recently reported Bose polarons [21–25]. However, an impurity in a bosonic bath just above the condensation threshold bears similarities with impurities immersed in an ultracold Fermi gas [17,26], as many wave vectors contribute to collisions. Using Ramsey spectroscopy, we monitor both the coherent interaction-induced frequency shift on the coherent superposition and the nonequilibrium decoherence of the probes. The level of individual atoms in this scheme allows realizing such quantum probing while minimizing perturbation of the bath. Thanks to comparison to a microscopic model, including precise knowledge of the molecular two-body interaction potential providing scattering cross sections [27], we demonstrate the capability for single-atom quantum probing via coherent or dephasing signals in ultracold gases.

The microscopic mechanism of our probing scheme is illustrated in Figs. 1(b)–1(d). In the regime of ultracold temperatures probed in this Letter, the interaction strength between Rb and Cs is only described by the s-wave scattering length a. For a given scattering length a_i between the impurity state $|i\rangle$ and the Rb cloud, the interaction energy writes $E_i = 2\pi\hbar^2 n a_i/\mu$, where n is the Rb density, μ is the reduced mass, and $\hbar$ is the reduced Planck constant. It leads to a time-dependent phase shift of the coherent superposition $(|g\rangle + ie^{i\Phi(t)}|e\rangle)/\sqrt{2}$ of the probe with phase [28]

$$\Phi(t) = \delta_{\mathrm{Rb}} t = \frac{2\pi\hbar^2 n \Delta a}{\mu\hbar} t, \tag{1}$$

where Δa is the difference of scattering lengths between excited $|e\rangle$ and ground $|g\rangle$ states $\Delta a = a_e - a_g$, leading to an interaction-induced energy shift $\hbar\delta_{\mathrm{Rb}}$ between the two impurity clock states. The information connected to density and temperature in this phase shift can be inferred from the phase and decoherence of the Ramsey signal after interaction time t as explained below. We enhance the sensitivity of the Ramsey phase to temperature by tuning the scattering length a_g close to the maximum of an interspecies Feshbach resonance. By contrast, the scattering length a_e is only slightly changing throughout this Letter and we assume a_e to be constant in the following. At the low-magnetic-field value close to the resonance, a_g changes significantly for changing collisional, i.e., kinetic, energy in an interatomic collision [29], see Fig. 1(b). For an ensemble at temperature T with a fixed magnetic field close to the resonance, thermal averaging leads to a temperature-dependent distribution of collision energies E_c according to a Maxwell-Boltzmann (MB) distribution [30]

$$p_{\mathrm{MB}}(E_c, T) = \frac{2\pi}{(\pi k_B T)^{3/2}} \sqrt{E_c} \exp\left(-\frac{E_c}{k_B T}\right). \tag{2}$$

This distribution translates into a distribution of scattering lengths, see Fig. 1(c). The resulting mean scattering length, see Fig. 1(d), drives the evolution of the interaction-induced phase shift of the impurity's superposition, which can be read out from our Ramsey-type scheme. The width of the scattering-length distribution leads to decoherence of the Ramsey signal through thermal averaging [31]. This effect can be understood in analogy with interference from a spectrally broad light source in optics. Additionally, the inhomogeneous density profile leads to a spatial dependence of the phase shift of the probe. As a consequence, the phase evolution of the impurity evolves faster in the center of the Rb cloud than in the wings, which modifies the Ramsey signal for varying peak densities. Thereby, the Ramsey-fringe signals allow determining of thermal properties of the bath from coherent evolution and dephasing dynamics of a single-atom probe. For fixed density, the comparison between mean value and the width of the scattering-length distribution allows for distinguishing two cases. First, for widths much smaller than the mean scattering length, dephasing emerges on a timescale longer than the inverse angular frequency of the Bloch vector precession on the Bloch sphere equator. In this configuration, the Ramsey-type interference signal will show a coherent phase shift of the Bloch vector. By contrast, for large widths of the scattering-length distribution, the Bloch vector dephases before completing a single revolution. In this case, the coherent phase shift cannot be reliably detected, but equivalent information can be extracted from the dephasing.

Experimentally, we prepare up to ten Cs impurities in the hyperfine ground state $|F_{\mathrm{Cs}} = 3, m_{F,\mathrm{Cs}} = 0\rangle$ at a temperature of $T_{\mathrm{Cs}} = 1.7$ μK and immerse them in a Rb bath. The number of ten Cs atoms is a compromise between enhancing the signal-to-noise ratio of measurements while keeping the probability of Cs-Cs interactions low. The limit of single atoms can be realized; however, the use of additional lattice potentials allows us to completely isolate the Cs atoms from each other. The Rb bath is prepared in state $|F_{\mathrm{Rb}} = 1, m_{F,\mathrm{Rb}} = 1\rangle$, where F_j and $m_{F,j}$ are the total atomic angular momentum and its projection onto the quantization axis for species j = Cs or Rb, respectively. The Rb cloud is produced with temperatures and peak densities in the range of $T = 200$–1000 nK and $n_0 = 0.2\times10^{13}$–2×10^{13} cm^{-3}, respectively. A high density-density overlap between impurity and Rb gas is achieved, because for the optical-trap wavelength of 1064 nm, Rb and Cs experience the same trap frequencies up to a few percent, leading to a negligible gravitational sag; the thermalized noninteracting distributions have a high overlap, which is further increased, because the Cs impurity becomes diffusive and effectively samples the Rb density distribution, see [32,33]. After thermalization, the two distributions can thus be considered identical for the gas densities used here. Thereafter, the Ramsey sequence [see Fig. 2(a)] is initialized on the clock transition $|g\rangle = |F_{\mathrm{Cs}} = 3, m_{F,\mathrm{Cs}} = 0\rangle \rightarrow |e\rangle = |F_{\mathrm{Cs}} = 4, m_{F,\mathrm{Cs}} = 0\rangle$

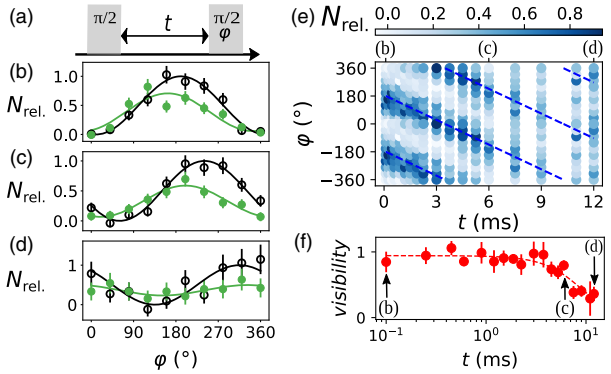

FIG. 2. (a) Ramsey sequence with waiting time t and adjustable phase φ of the last pulse. Ramsey fringes for (b) $t = 0.1$, (c) $t = 6$, and (d) $t = 12$ ms for the case without (black, open circles) and with (green, filled circles) Rb bath. (e) Time evolution of the color-coded Ramsey signal for a bath peak density of $n_{\mathrm{Rb}} = 0.195 \times 10^{13}\,\mathrm{cm}^{-3}$ and temperature of $T = 980$ nK, showing the phase evolution. The phase shift is directly proportional to evolution time, where the slope is given by the energy difference between the two Cs clock states. The dashed line is a linear fit to the fringe maxima; the negative phase is a copy of positive phase data for better illustration. (f) Decay of Ramsey-fringe contrast with time. The decoherence time T_2 is fitted by a Gaussian function.

by a first microwave $\pi/2$ pulse with Rabi frequency $\Omega_0 = 2\pi \times 15.4$ kHz, preparing the coherent state $|\psi(0)\rangle = (1/\sqrt{2})(|g\rangle + i|e\rangle)$. During a free-evolution time t the superposition acquires a phase $|\psi(t)\rangle = (1/\sqrt{2})(|g\rangle + ie^{i\Delta\times t}|e\rangle)$, where $\hbar\Delta$ is the total energy difference between the Cs clock states. It contains differential light shifts and the second-order Zeeman shift, as well as the interaction-induced shift $\hbar\delta_{\mathrm{Rb}}$. After an interaction time t between the impurity and the bath, a second $\pi/2$ pulse is applied with adjustable phase φ relative to the first pulse. To obtain the typical Ramsey fringe at a fixed time t [see Figs. 2(b)–2(d)], we measure the population in state $|g\rangle$ (see the Supplemental Material [33]) for the full phase range of $\varphi = 0° - 360°$. Each measured Ramsey fringe represents the ensemble average of approximately 10^3 atoms. Figure 2(e) shows the full time evolution. A species-selective lattice allows one to obtain spatial resolution along the axial direction to select those Cs atoms spatially overlapping with the Rb cloud. The measured population in $|F = 3\rangle$ after the Ramsey sequence is fitted by

$$p(t,\varphi) = \frac{1}{2} + \left(\sin^2\left[\frac{\Delta \times t - \varphi}{2}\right] - \frac{1}{2}\right)\exp\left[-\frac{t^2}{T_2^2}\right], \qquad (3)$$

where we have added phenomenological Gaussian dephasing with dephasing time T_2. In order to analyze the data, we normalize each fringe to obtain relative numbers (see [33]) and fit the fringes with a function $A\sin^2[(\phi - \varphi)/2] + C$, with amplitude A, offset C, and fringe phase ϕ. From amplitude and offset, we deduce the fringe visibility, for each t, as $\mathcal{V} = (p_{\max} - p_{\min})/(p_{\max} + p_{\min}) = A/(A + 2C)$. From the difference in contrast for measurements with and without Rb cloud, we determine the interaction-induced visibility loss as a measure of dephasing, see Fig. 2(f). The T_2 time is now extracted with a Gaussian fit to the visibility

$$\mathcal{V}(t) = \mathcal{V}_0 \exp\left(-\frac{t^2}{T_2^2}\right) + B, \qquad (4)$$

with amplitude $\mathcal{V}_0$ and offset B. The offset is due to residual Cs atoms noninteracting with the Rb cloud. To extract only the interaction-induced phase for every free-evolution time t [see Fig. 3(a)], we subtract the contributions of interaction with the environment besides the bath interaction, as $\Phi(t) = \phi(t) - \delta_{\mathrm{bg}}t$, with δ_{bg} as the background phase shift without the Rb bath. The dominating contributions to δ_{bg} are the differential light shift δ_{DT} of the dipole trap (DT) and the second-order Zeeman shift δ_B [33]. We find with an independent characterization $\delta_{\mathrm{bg}} = \delta_{\mathrm{DT}} + \delta_B \approx -2\pi \times 135$ Hz for a Cs temperature of $T_{\mathrm{Cs}} = 1.7\ \mu$K. We use this value throughout the analysis, neglecting small changes of the detuning for reduced temperatures of the Cs atoms [47]. The dephasing T_2 time without Rb has been measured to be $T_2 = 27.2$ ms and is therefore neglected [33].

We first probe the gas density information at a temperature of $T = 850$ nK, as shown in Fig. 3, where the dephasing is sufficiently small to monitor the phase evolution [33]. We record Ramsey fringes for variable interaction times with and without a Rb bath and extract the interaction-induced phase shift dynamics and contrast decay. For a given parameter set, the phase difference shows a linear change with time, where the slope is given by the interaction-induced detuning δ_{Rb}. In addition, we extract the dephasing time T_2 as in Eq. (4). For the dephasing times T_2 extracted, we find a reduced dephasing time T_2 for increasing density as shown in Fig. 3(b).

We compare our data to a model without free parameters, computing the expectation value of Ramsey fringes with thermal and density averaging. It takes the standard form of a Ramsey fringe with collisional phase shift Eq. (1), which depends on density and collisional-energy-dependent scattering length. We average the signal using the density distribution $p_{\mathrm{Rb}}(\vec{r})$ [33] and Maxwell-Boltzmann distribution (2) as distribution functions

$$p(t,\varphi) = \int_0^\infty \int_V p_{\mathrm{Rb}} \cos^2\left(\frac{\delta_{\mathrm{Rb}}t}{2} - \frac{\varphi}{2}\right) dV\, p_{\mathrm{MB}}\, dE_c, \qquad (5)$$

with $\delta_{\mathrm{Rb}} \propto n(\vec{r})\Delta a(E_c)$. Here, we assume thermalization of the Cs atoms with the bath, so that the radial impurity distribution takes the form of the bath distribution, allowing us to model the density-density overlap only via the Rb density distribution. A detailed discussion on the analytical

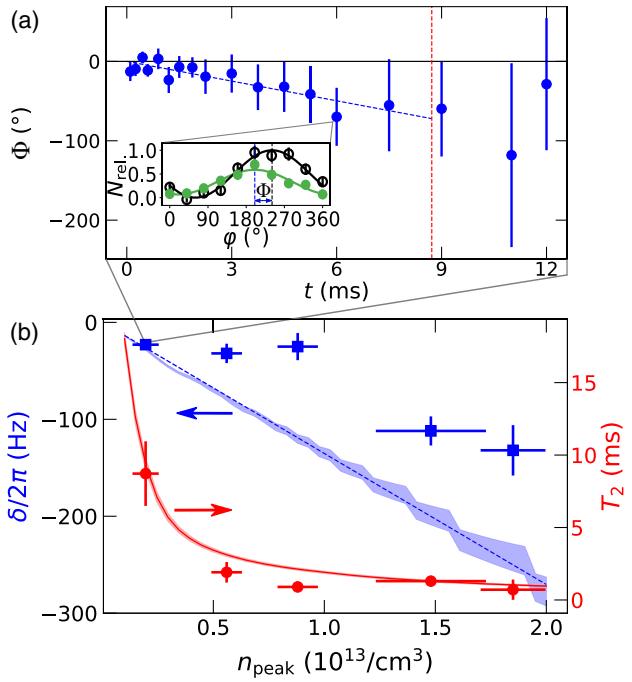

FIG. 3. (a) Interaction-induced phase shift $\Phi(t)$ as a function of free-evolution time t. The data are fitted with a line (dashed blue line) to extract the slope δ up to the dephasing time T_2, indicated by the vertical dashed line. Inset: a Ramsey fringe for $t = 6$ ms with (green, filled circles) and without (black, open circles) Rb cloud. (b) Measured interaction-induced detuning δ (blue data points) and T_2 times (red data points) as a function of gas density. The red solid and blue dashed lines are predictions of Eq. (5) without free parameter. The fixed temperature $T = 850$ nK with changing density leads, in this dataset, to a range of $T/T_c = 2.2, \ldots, 5$ for the Rb gas.

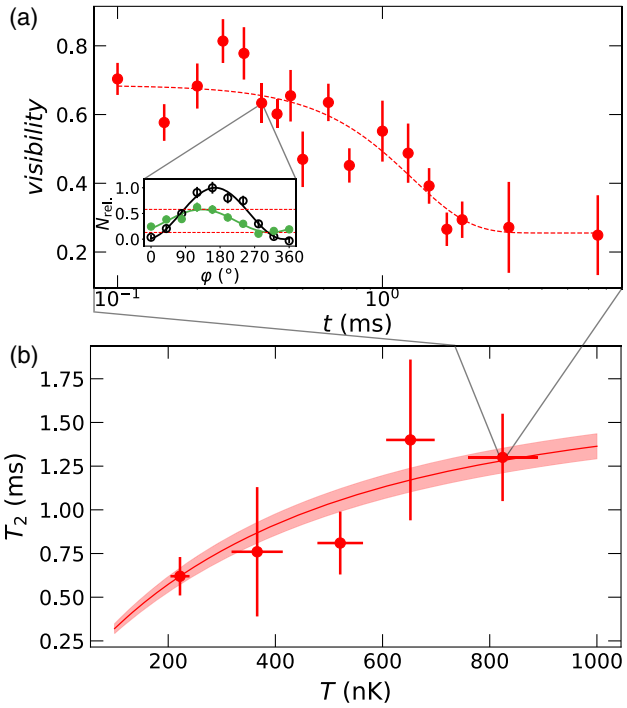

FIG. 4. (a) Decay of the Ramsey-fringe contrast as a function of evolution time in the Rb bath. The dashed line is a Gaussian fit. Inset: Ramsey fringes for $t = 0.6$ ms for Cs atom without (black, open) and with (green, filled) Rb bath present. (b) Dephasing time of impurities in the Rb bath as a function of gas temperature. The data (red points) show an increase with temperature; the red line is a prediction of our model. Data are taken for a fixed Rb peak density of $n_{\mathrm{Rb}} \approx 1.5 \times 10^{13}$ cm^{-3}. Error bars and shaded area indicate 1σ uncertainties of the experimental data and numerical model, respectively. Scaled with the critical temperature, the temperature range is $T/T_c = 1.2$–2.3.

model for the averaged Ramsey signal, including an additional Monte Carlo simulation, is given in the Supplemental Material [33]. We analyze the numerical signals by the same procedure as the experimental ones to obtain the mean phase shift δ and the dephasing time T_2. While the phase evolution shows qualitatively similar behavior between our experimental data and our model, but quantitative differences, we find good agreement for the dephasing. We note that the coherence times of few milliseconds is not sufficient to reliably measure phase shifts of a few 100 Hz, which can explain the quantitative discrepancy between measurement and model. This supports our assumption that the Rb bath's inhomogeneous density dominates the dephasing at this temperature. We emphasize that both theory lines in Fig. 3(b) originate from the same parameter-free model, Eq. (5). We conclude that phase shift and decoherence both reflect the atomic peak density.

Second, we study the nonequilibrium dephasing of the coherent superposition as a probe for the temperature of the Rb cloud, following the spirit of Ref. [20]. When probing the temperature of the gas, we find that the phase shift cannot be reliably extracted from the data for low temperatures, as expected. Instead, we use the decoherence and measure the characteristic coherence time T_2 to obtain information about the temperature of the gas and compare it with the independently measured gas temperature via time-of-flight velocimetry. Figure 4 shows the measured T_2 time as a function of temperature, with the visibility fitted using Eq. (4). The temperature dependence of the T_2 time is only due to the dependence of the collision energy of the scattering length, since the peak density is constant.

We find a good agreement between the experimental data and our parameter-free model. We emphasize here that the temperature axis in Fig. 4(b) indicates time-of-flight temperatures of the gas, where the numerical model has assumed thermalization of the Cs impurity with the cloud. Thus, our results demonstrate that temperature information can be obtained from the dephasing Ramsey signal of individual impurities coupled to a gas.

The ability to use the coherent and decoherence dynamics of the superposition states of a single-impurity probe brings probing of a many-body system to the quantum level. An interesting question concerns the degree of

perturbation of the measurement on the many-body system. Elastic collisions do not modify the energy distribution of the gas. Still, the information written in the phase of the quantum superposition leads to an entanglement between the many-body system and the probe. This can be illustrated by considering the nominal number of collisions, which the probe undergoes during the coherence time in each spin state. For Cs state $|g\rangle$ ($|e\rangle$), it is in the range of 6–18 (0.4–1.8), reflecting the strongly differing scattering cross sections close to the Feshbach resonance and leading to a probe-state-dependent redistribution of energies in the microscopic configuration of the gas. For a classical gas, the perturbation of the many-body system following a measurement on the probe cannot be inferred. In the future, it will be interesting to prepare the gas in a Bose-Einstein condensate, where the entanglement between probe and system is restricted to a single mode in the quantum gas, and the perturbation of the gas at the level of perturbation at the Heisenberg limit might be detected. Here, also the decoherence dynamics for baths in reduced dimensions, with spin degree of freedom, or in nonequilibrium states can be inferred. Although our method assumes knowledge on the quantum state of the system, it paves the way using universal and model-independent coherent interferometry schemes, through, e.g., fluctuation dissipation theorems [14].

We thank E. Tiemann for providing us with the energy-dependent scattering lengths for Rb-Cs collisions, and I. Schneider and M. Fleischhauer for helpful discussions on the decoherence models. We acknowledge helpful discussions with Thomas Busch and Miguel Garcia-March, which helped us improving the presentation. S. B. acknowledges funding by the Studienstiftung des deutschen Volkes. This work was supported by Deutsche Forschungsgemeinschaft (DFG) via Sonderforschungsbereich SFB/TRR 185, Project No. 277625399.

*widera@physik.uni-kl.de

[1] D. Tamascelli, C. Benedetti, H.-P. Breuer, and M. G. A. Paris, Quantum probing beyond pure dephasing, New J. Phys. **22**, 083027 (2020).

[2] T. J. Elliott and T. H. Johnson, Nondestructive probing of means, variances, and correlations of ultracold-atomic-system densities via qubit impurities, Phys. Rev. A **93**, 043612 (2016).

[3] A. Usui, B. Buča, and J. Mur-Petit, Quantum probe spectroscopy for cold atomic systems, New J. Phys. **20**, 103006 (2018).

[4] F. M. Spiegelhalder, A. Trenkwalder, D. Naik, G. Hendl, F. Schreck, and R. Grimm, Collisional Stability of ^{40}K Immersed in a Strongly Interacting Fermi Gas of ^{6}Li, Phys. Rev. Lett. **103**, 223203 (2009).

[5] R. Olf, F. Fang, G. E. Marti, A. MacRae, and D. M. Stamper-Kurn, Thermometry and cooling of a Bose gas to 0.02 times the condensation temperature, Nat. Phys. **11**, 720 (2015).

[6] R. S. Lous, I. Fritsche, M. Jag, B. Huang, and R. Grimm, Thermometry of a deeply degenerate Fermi gas with a Bose-Einstein condensate, Phys. Rev. A **95**, 053627 (2017).

[7] M. Hohmann, F. Kindermann, T. Lausch, D. Mayer, F. Schmidt, and A. Widera, Single-atom thermometer for ultracold gases, Phys. Rev. A **93**, 043607 (2016).

[8] Q. Bouton, J. Nettersheim, D. Adam, F. Schmidt, D. Mayer, T. Lausch, E. Tiemann, and A. Widera, Single-Atom Quantum Probes for Ultracold Gases Boosted by Non-equilibrium Spin Dynamics, Phys. Rev. X **10**, 011018 (2020).

[9] H. T. Ng and S. Bose, Single-atom-aided probe of the decoherence of a Bose-Einstein condensate, Phys. Rev. A **78**, 023610 (2008).

[10] A. Klein, M. Bruderer, S. R. Clark, and D. Jaksch, Dynamics, dephasing and clustering of impurity atoms in Bose-Einstein condensates, New J. Phys. **9**, 411 (2007).

[11] L. A. Correa, M. Mehboudi, G. Adesso, and A. Sanpera, Individual Quantum Probes for Optimal Thermometry, Phys. Rev. Lett. **114**, 220405 (2015).

[12] D. Hangleiter, M. T. Mitchison, T. H. Johnson, M. Bruderer, M. B. Plenio, and D. Jaksch, Nondestructive selective probing of phononic excitations in a cold Bose gas using impurities, Phys. Rev. A **91**, 013611 (2015).

[13] G. L. Giorgi, F. Galve, and R. Zambrini, Probing the spectral density of a dissipative qubit via quantum synchronization, Phys. Rev. A **94**, 052121 (2016).

[14] T. H. Johnson, F. Cosco, M. T. Mitchison, D. Jaksch, and S. R. Clark, Thermometry of ultracold atoms via non-equilibrium work distributions, Phys. Rev. A **93**, 053619 (2016).

[15] F. Cosco, M. Borrelli, F. Plastina, and S. Maniscalco, Momentum-resolved and correlation spectroscopy using quantum probes, Phys. Rev. A **95**, 053620 (2017).

[16] H. Edri, B. Raz, N. Matzliah, N. Davidson, and R. Ozeri, Observation of Spin-Spin Fermion-Mediated Interactions between Ultracold Bosons, Phys. Rev. Lett. **124**, 163401 (2020).

[17] M. Cetina, M. Jag, R. S. Lous, I. Fritsche, J. T. M. Walraven, R. Grimm, J. Levinsen, M. M. Parish, R. Schmidt, M. Knap, and E. Demler, Ultrafast many-body interferometry of impurities coupled to a Fermi sea, Science **354**, 96 (2016).

[18] M. Mehboudi, A. Sanpera, and L. A. Correa, Thermometry in the quantum regime: Recent theoretical progress, J. Phys. A **52**, 303001 (2019).

[19] M. Mehboudi, A. Lampo, C. Charalambous, L. A. Correa, M. A. García-March, and M. Lewenstein, Using Polarons for Sub-nk Quantum Nondemolition Thermometry in a Bose-Einstein Condensate, Phys. Rev. Lett. **122**, 030403 (2019).

[20] M. T. Mitchison, T. Fogarty, G. Guarnieri, S. Campbell, T. Busch, and J. Goold, In Situ Thermometry of a Cold Fermi Gas via Dephasing Impurities, Phys. Rev. Lett. **125**, 080402 (2020).

[21] Z. Z. Yan, Y. Ni, C. Robens, and M. W. Zwierlein, Bose polarons near quantum criticality, Science **368**, 190 (2020).

[22] N.-E. Guenther, P. Massignan, M. Lewenstein, and G. M. Bruun, Bose Polarons at Finite Temperature and Strong Coupling, Phys. Rev. Lett. **120**, 050405 (2018).

[23] W. E. Liu, J. Levinsen, and M. M. Parish, Variational Approach for Impurity Dynamics at Finite Temperature, Phys. Rev. Lett. **122**, 205301 (2019).
[24] D. Dzsotjan, R. Schmidt, and M. Fleischhauer, Dynamical Variational Approach to Bose Polarons at Finite Temperatures, Phys. Rev. Lett. **124**, 223401 (2020).
[25] M. G. Skou, T. G. Skov, N. B. Jorgensen, K. K. Nielsen, A. Camacho-Guardian, T. Pohl, G. M. Bruun, and J. J. Arlt, Non-equilibrium quantum dynamics and formation of the Bose polaron, Nat. Phys. **17**, 731 (2021).
[26] R. Schmidt, M. Knap, D. A. Ivanov, J.-S. You, M. Cetina, and E. Demler, Universal many-body response of heavy impurities coupled to a Fermi sea: A review of recent progress, Rep. Prog. Phys. **81**, 024401 (2018).
[27] F. Schmidt, D. Mayer, Q. Bouton, D. Adam, T. Lausch, J. Nettersheim, E. Tiemann, and A. Widera, Tailored Single-Atom Collisions at Ultralow Energies, Phys. Rev. Lett. **122**, 013401 (2019).
[28] F. Schmidt, D. Mayer, Q. Bouton, D. Adam, T. Lausch, N. Spethmann, and A. Widera, Quantum Spin Dynamics of Individual Neutral Impurities Coupled to a Bose-Einstein Condensate, Phys. Rev. Lett. **121**, 130403 (2018).
[29] E. L. Bolda, E. Tiesinga, and P. S. Julienne, Effective-scattering-length model of ultracold atomic collisions and Feshbach resonances in tight harmonic traps, Phys. Rev. A **66**, 013403 (2002).
[30] M. Cannoni, Relativistic $\langle \sigma v_{\mathrm{rel}} \rangle$ in the calculation of relics abundances: A closer look, Phys. Rev. D **89**, 103533 (2014).
[31] W. Yang, W.-L. Ma, and R.-B. Liu, Quantum many-body theory for electron spin decoherence in nano-scale nuclear spin baths, Rep. Prog. Phys. **80**, 016001 (2016).
[32] M. Hohmann, F. Kindermann, T. Lausch, D. Mayer, F. Schmidt, E. Lutz, and A. Widera, Individual Tracer Atoms in an Ultracold Dilute Gas, Phys. Rev. Lett. **118**, 263401 (2017).
[33] See Supplemental Material at http://link.aps.org/supplemental/10.1103/PhysRevLett.129.120404 for experimental details, including Refs. [34–46].
[34] D. Mayer, F. Schmidt, S. Haupt, Q. Bouton, D. Adam, T. Lausch, E. Lutz, and A. Widera, Nonequilibrium thermodynamics and optimal cooling of a dilute atomic gas, Phys. Rev. Research **2**, 023245 (2020).
[35] W. Alt, D. Schrader, S. Kuhr, M. Müller, V. Gomer, and D. Meschede, Single atoms in a standing-wave dipole trap, Phys. Rev. A **67**, 033403 (2003).
[36] F. Schmidt, D. Mayer, M. Hohmann, T. Lausch, F. Kindermann, and A. Widera, Precision measurement of the ^{87}Rb tune-out wavelength in the hyperfine ground state $f = 1$ at 790 nm, Phys. Rev. A **93**, 022507 (2016).
[37] D. Mayer, F. Schmidt, D. Adam, S. Haupt, J. Koch, T. Lausch, J. Nettersheim, Q. Bouton, and A. Widera, Controlled doping of a bosonic quantum gas with single neutral atoms, J. Phys. B **52**, 015301 (2018).
[38] B. Butscher, J. Nipper, J. Balewski, L. Kukota, V. Bendkowsky, R. Low, and T. Pfau, Atom-molecule coherence for ultralong-range Rydberg dimers, Nat. Phys. **6**, 970 (2010).
[39] P. Del Moral, *Mean Field Simulation for Monte Carlo Integration* (Chapman and Hall/CRC, New York, 2013), pp. 1–575.
[40] W. K. Hastings, Monte Carlo sampling methods using Markov chains and their applications, Biometrika **57**, 97 (1970).
[41] J. Goold, T. Fogarty, N. Lo Gullo, M. Paternostro, and T. Busch, Orthogonality catastrophe as a consequence of qubit embedding in an ultracold Fermi gas, Phys. Rev. A **84**, 063632 (2011).
[42] M. Knap, A. Shashi, Y. Nishida, A. Imambekov, D. A. Abanin, and E. Demler, Time-Dependent Impurity in Ultracold Fermions: Orthogonality Catastrophe and beyond, Phys. Rev. X **2**, 041020 (2012).
[43] H.-P. Breuer and F. Petruccione, *The Theory of Open Quantum Systems* (Oxford University Press, New York, 2002).
[44] N. B. Jørgensen, L. Wacker, K. T. Skalmstang, M. M. Parish, J. Levinsen, R. S. Christensen, G. M. Bruun, and J. J. Arlt, Observation of Attractive and Repulsive Polarons in a Bose-Einstein Condensate, Phys. Rev. Lett. **117**, 055302 (2016).
[45] S. Chapman and T. G. Cowling, *The Mathematical Theory of Non-Uniform Gases* (Cambridge University Press, Cambridge, England, 1953), p. 448.
[46] J. E. Runeson and J. O. Richardson, Quantum Entanglement from Classical Trajectories, Phys. Rev. Lett. **127**, 250403 (2021).
[47] S. Kuhr, W. Alt, D. Schrader, I. Dotsenko, Y. Miroshnychenko, A. Rauschenbeutel, and D. Meschede, Analysis of dephasing mechanisms in a standing-wave dipole trap, Phys. Rev. A **72**, 023406 (2005).